

Direct temperature determination of a sympathetically cooled large $^{113}\text{Cd}^+$ ion crystal for a microwave clock

Y. N. Zuo,^{1,2} J. Z. Han,^{1,2} J. W. Zhang,^{2,3, a)} and L. J. Wang^{1,2,3, b)}

¹⁾*Department of Physics, Tsinghua University, Beijing 100084, China*

²⁾*State Key Laboratory of Precision Measurement Technology and Instruments, Tsinghua University, Beijing 100084, China*

³⁾*Department of Precision Instruments, Tsinghua University, Beijing 100084, China*

(Dated: 14 January 2022)

This paper reports direct temperature determination of sympathetically cooled $^{113}\text{Cd}^+$ ions with laser-cooled $^{24}\text{Mg}^+$ in a linear Paul trap. The sympathetically cooled ion species distribute in the outer shell of the large ensembles, which contain up to 3.3×10^5 ions. With optimized parameters, the minimum temperature of the sympathetically cooled $^{113}\text{Cd}^+$ ions was measured to be on the order of 10 mK. These results are promising for performance of microwave atomic clocks. The second-order Doppler frequency shift is two orders of magnitudes lower (from 1.88×10^{-14} to 6.26×10^{-16}) and the Dick effect is suppressed.

Charged particles in ion traps are more strongly bound than neutral atoms in magneto-optical traps. With lasers, trapped ions can be cooled translationally by Doppler cooling only to the millikelvin level, and need further cooling down to the vibrational ground state on the microkelvin scale.^{1,2} Hence, ion trapping is used widely in precision measurements, such as frequency metrology,¹ mass spectrometry,³ precision spectroscopy,⁴ quantum information processing,⁵ measuring physical constants,⁶ and chemical physics.⁷ Frequency standards based on trapped ions play an important role in frequency metrology. In particular, microwave frequency standards based on ions have good potential for use in compact atomic clocks,^{8–10} deep-space navigation, ultra-stable time-keeping, and space-borne clocks.¹¹

The microwave clock based on laser-cooled $^{113}\text{Cd}^+$ had a short-term frequency instability of $6.1 \times 10^{-13}/\sqrt{\tau}$ and a frequency uncertainty of 6.6×10^{-14} .¹² Nevertheless, it has not reached the performance anticipated by Zhang *et al.*¹³ This kind of microwave frequency standard, based on laser-cooled ions, generally suffers from the Dick effect owing to the dead time for the operation and the second-order Doppler frequency shift (SODFS) from ion temperature rising during the clock interrogated.¹⁴ Sympathetic cooling (SC) is promising for overcoming both of these limitations. SC can cool the translational motion of the target atomic or molecular ions via mutual Coulomb interaction. It was first realized for isotopic ions in a Penning trap.¹⁵ It has been demonstrated with laser-cooled alkaline-earth and alkaline-like-earth metal ions, such as Be^+ , Mg^+ , Ca^+ , Ba^+ , and Yb^+ . The Doppler limit (<1 mK) has been reached for small crystals consisting of about 10 ions, as verified by spatial thermometry.¹⁶ By applying SC, the temperature of Cd^+ ions can be kept low during the whole interrogation sequence, and no additional cooling is needed. Because the ion temperature is low, the SODFS and uncertainty in SODFS due to ion motion can be significantly reduced. Moreover, the Dick effect can be suppressed because the dead time is shorter than for a directly cooled Cd^+ clock.

We have proposed using $^{24}\text{Mg}^+$ as the coolant to sympathetically cool a large $^{113}\text{Cd}^+$ cloud.¹⁷ In contrast with other ions, $^{24}\text{Mg}^+$ only needs one laser to cool it. The large mass difference between the Cd^+ and Mg^+ ions (mass ratio = 4.71) results in a significant spatial separation between these two kinds of ion crystal, which is helpful for reducing the AC Stark shift caused by laser cooling the $^{24}\text{Mg}^+$ ions. To estimate the SODFS, the exact temperature of $^{113}\text{Cd}^+$ has to be obtained. One can measure the Doppler broadening of a spectral transition to determine the ion temperature.^{18–20} However, it is difficult to measure the ion temperature directly without suitable direct-cooling lasers. An indirect method for measuring the ion temperature is to compare CCD photographs of the ions to statistical images generated by a molecular dynamics (MD) simulation.²¹ Nevertheless, the accuracy of this method is limited by the hypotheses used in the simulation models and the computational accuracy. There are several reports of direct measurements of SC ion temperature. For example, Wineland *et al.* measured the temperature of $^{199}\text{Hg}^+$ sympathetically cooled by $^9\text{Be}^+$ in Penning traps to 0.4–1.8 K,²² and Imajo *et al.* measured the temperature of SC Cd^+ cooled to 1 K using isotopic ions, also in Penning traps.²³ The direct temperature of the inner Mg^+ core of Ca^+-Mg^+ bi-crystals was measured as 40 mK in a Paul trap.¹⁸ Reported experiments show that it is very challenging to cool target ions sympathetically using coolant ions with large mass differences because of the limited cooling efficiency.²⁴

In this letter, we report the direct temperature measurement of $^{113}\text{Cd}^+$ sympathetically cooled by $^{24}\text{Mg}^+$. This can be used in a highly accurate microwave atomic clock. The temperature of the outer shell of a sympathetically cooled ion crystal was directly measured to be on the sub-kelvin scale with as many as 3.3×10^5 ions and a large mass ratio in a Paul trap. The SODFS was reduced to two orders of magnitude lower than that of laser-cooled ion clouds.¹² Moreover, the Dick effect was also reduced owing to a shorter dead time, because no additional cooling was needed. Hence, this makes it possible to build high-performance microwave atomic clocks based on SC ions. This result can also be treated as an upper limit for the translational temperature of outer-shell SC ions when refining MD simulation models.

^{a)}Electronic mail: zhangjw@mail.tsinghua.edu.cn

^{b)}Electronic mail: lwan@mail.tsinghua.edu.cn

The experimental setup was an enhanced version of that described in previous reports.^{12,13} We used a linear quadrupole Paul trap made of oxygen-free copper. It had four parallel cylindrical electrodes each with a radius of $r_e = 7.1$ mm. Each electrode was divided into three segments, of lengths 20, 40, and 20 mm. The minimum distance from the trap center axis to the surfaces of the electrodes was $r_0 = 6.2$ mm. The ratio of r_e to r_0 was close to the optimized value for an ideal quadrupole field.²⁵ A radio frequency (RF) voltage V_{RF} was applied to one pair of diagonal electrodes, and the other pair was grounded. The driving frequency was $\Omega = 2\pi \times 2.02$ MHz. A static voltage U_{End} was added to the end-cap electrodes, which could be adjusted between 0 and 120 V to manipulate the shapes of the Coulomb crystals. The trapping parameters²⁶ of the well-known Mathieu equation are $q_r^{\text{Mg}} = 0.03$ and $q_r^{\text{Cd}} = 0.15$, and the trap depths are $d^{\text{Mg}} = 2.11$ eV and $d^{\text{Cd}} = 0.45$ eV.

To manipulate the Cd^+ and Mg^+ at the same time, two frequency-quadrupled lasers with wavelengths of 214 and 280 nm counter-propagated along the trap axis. The diameters of the two laser beams were both 1 mm, and the intensities were 6 mW/mm^2 at 280 nm and 1 mW/mm^2 at 214 nm. The frequencies were stabilized with high-precision wavemeters at the transition lines of $3s^2S_{1/2} \leftrightarrow 3p^2P_{1/2}$ of $^{24}\text{Mg}^+$ and $5s^2S_{1/2} \leftrightarrow 5p^2P_{3/2}$ of $^{113}\text{Cd}^+$. The natural width the D_1 line for $^{24}\text{Mg}^+$ is $2\pi \times 42.7$ MHz, which gives a minimum Doppler temperature of 1.0 mK,²⁷ while the natural width of the D_2 line for $^{113}\text{Cd}^+$ is $2\pi \times 60.1$ MHz, corresponding to 1.4 mK.²⁸ The ions were imaged by an electron-multiplying charge-coupled device (EMCCD) camera. The camera system, which was mounted on a precision motion stage, consisted of a lens system, tunable pinhole, and ultraviolet (UV) filters. The magnification factor of the lens could be adjusted from 4 to 8. The exposure time was set to 0.3 seconds for one shot. In addition, we used a photo-multiplier tube with optional filters at the opposite side of the trap axis to monitor the fluorescence intensity.

To load the ions, neutral atoms were evaporated from pure metal in different ovens. The ^{24}Mg isotope was at the natural abundance, while ^{113}Cd was isotopically enriched. Magnesium atoms were ionized by electron bombardment, and cadmium atoms were ionized by resonance-enhanced two-photon ionization using another frequency-quadrupled laser at 228 nm. Photo-ionization for $^{113}\text{Cd}^+$ avoids disturbing and heating the loaded Mg^+ .¹⁸ Photo-ionization further has the advantages of a controllable high loading efficiency and isotopic selection, and it does not produce a stray electric field like that from the residual charge of an electron gun. The Mg^+ ions were loaded first, and the Cd^+ ions were then loaded. The ionization energy was set to avoid production of $^{24}\text{Mg}^{2+}$, whose ionization energy is 22.7 eV.^{18,29} While loading Mg^+ , V_{RF} was set to a higher value than for normal detection to produce a deeper potential depth to load more ions. The compensation voltages applied to the electrodes have to be tuned carefully after loading to obtain symmetric ion crystals. During the loading, many of the $^{24}\text{Mg}^+$ ions are converted to $^{24}\text{MgH}^+$ dark molecular ions through chemical reactions with residual H_2 molecules in the background gas,³⁰ which reduces the

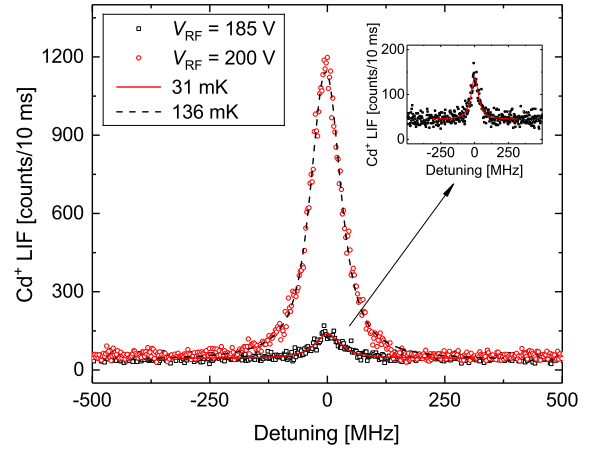


FIG. 1. Fluorescence spectrum of SC $^{113}\text{Cd}^+$. Experimental data are marked by squares and circles for $V_{\text{RF}} = 185$ V and 200 V, respectively. The curves are fitted with a Voigt function having a Lorentz linewidth of 60.13 MHz, which is the natural width of the D_2 transition of $^{113}\text{Cd}^+$. The temperatures obtained for $^{113}\text{Cd}^+$ are 31 mK and 136 mK, respectively. The inset shows the fitting of the 31 mK result.

number of ions and decreases SC efficiency. In contrast, the production rate of CdH^+ is quite low.

To determine the temperature of SC Cd^+ , we measured the Doppler broadening of the transition from $5s^2S_{1/2} F = 1$ to $5p^2P_{3/2} F = 2$. During this measurement, the intensity of the 214 nm laser was set to $20 \mu\text{W/mm}^2$ to avoid cooling or heating the ions. The frequency of 214 nm laser was scanned around the resonant frequency with a range of 1 GHz. The measured line profiles were fitted with a Voigt function. The Lorentz linewidth of the Voigt function was set as the natural linewidth of the D_2 transition of $^{113}\text{Cd}^+$, which is 60.13 MHz (2.647 ± 0.010 ns).²⁸ The Gaussian linewidth from the fitting represents the velocity distribution of the SC Cd^+ ions. Thus, the temperature can be calculated via^{31–33}

$$T = \frac{Mc^2}{8 \ln 2 \cdot k_B} \left(\frac{\Delta v_G}{v_0} \right)^2, \quad (1)$$

where M is the mass of $^{113}\text{Cd}^+$, c is the speed of light, k is the Boltzmann constant, Δv_G is the Gaussian linewidth, and v_0 is the resonant frequency of the D_2 transition of Cd^+ . Figure 1 shows a typical Voigt fitting of the laser-induced fluorescence (LIF) spectra. The LIF intensity is proportional to the number of resonant ions, and the ion temperature depends on V_{RF} and the number of ions. As shown in Fig. 1, the temperature is 136 mK when $V_{\text{RF}} = 200$ V and 31 mK when $V_{\text{RF}} = 185$ V. These results indicate that the ion temperature is sensitive to the variation of V_{RF} for SC when there is a large mass difference between the two ion species.

Ions with different charge-to-mass ratios have different displacements owing to the mass dependence of the pseudo-potential. In large multi-component Coulomb crystals, such displacements can result in a complete radial separation.²¹ Moreover, the different radiation pressures of the cooling

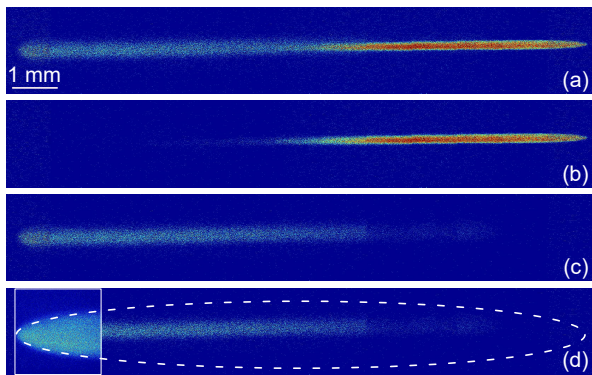


FIG. 2. Combination photographs of Cd^+ and Mg^+ captured by the EMCCD with UV filters and a 0.3 s exposure time. The total number of ions is $N_{\text{tot}} = 3.3 \times 10^5$. Each picture is a composite of 12 separate EMCCD photographs. Panel (a) is a composite of (b) and (c), with $V_{\text{RF}} = 280$ V and $U_{\text{End}} = 10$ V, where (b) and (c) show Mg^+ and Cd^+ , respectively. These two kinds of ions are pushed to different sides of the cloud owing to the unidirectional laser incidence. The small difference in the magnification factor due to the chromaticity is taken into account. The left end of (d), marked by the solid box, is obtained by overlaying 10 photographs taken for different positions of the laser beam for Cd^+ . The profile of the entire ion cloud is marked by the dashed line.

lasers segregates the ions axially. In Fig. 2, only the axial separation is clearly shown. A clear radial separation is shown in Fig. 3, which is for fewer ions than in Fig. 2.

We had to photograph the entire multi-component ion crystal to obtain its configuration and dimensions. The crystal had a large aspect ratio owing to the relatively weak axial confinement field. Because the diameter of the 214.5 nm laser beam was 1 mm, the diameters of the Cd^+ ion clouds were larger than those of the laser beams. Thus, only part of the Cd^+ could be imaged in a single exposure owing to the limited EMCCD image area. Composite photographs of the entire ion cloud can be obtained by stitching together 12 EMCCD photos, as shown in Fig. 2. Moreover, because of the lens chromaticity at 214.5 nm and 280 nm, the focus positions are different for Mg^+ and Cd^+ . This difference was taken account in combining the photographs.

The numbers of the two visible atomic ions were estimated using the size of the ion crystal in the EMCCD images and the calculated ion number density. Using the zero-temperature charged-liquid model,^{18,34} the number density $n_{0,i}$ under the pseudo-potential approximation is

$$n_{0,i}(r,z) = n_i = \frac{\epsilon_0 V_{\text{RF}}^2}{M_i \Omega^2 r_0^4}, \quad (2)$$

where i indicates the ion species, ϵ_0 is the permittivity of a vacuum, V_{RF} is the voltage applied to the electrodes, M_i is the ion mass, k is the Boltzmann's constant, and Ω is the trap driving frequency. Thus, the number densities for Mg^+ and Cd^+ are $n_{0,\text{Mg}} = 7.32 \times 10^{13} \text{ m}^{-3}$ and $n_{0,\text{Cd}} = 1.55 \times 10^{13} \text{ m}^{-3}$, respectively, with $V_{\text{RF}} = 280$ V.

To obtain the total number of ions in the multi-component crystal, we have to estimate the total volume of the ions.

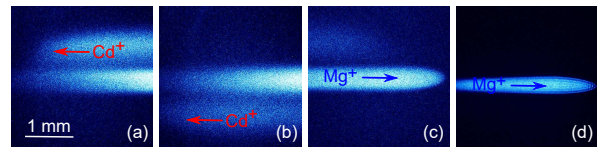


FIG. 3. EMCCD images of a multi-component ion crystal for a 3 s exposure time. Panels (a), (b), and (c) were taken simultaneously without UV filters. The red arrow indicates the propagating direction of the 214 nm laser, and the blue one is that for the 280 nm laser. Panel (d) is a clear EMCCD image of a $^{24}\text{Mg}^+$ ion crystal taken with a 280 nm filter.

The Mg^+ crystal in the core is approximated as a cylinder and the Cd^+ crystal as an ellipsoid shell. From Fig. 2, the three radii of the ellipsoid shell are 6.45 mm, 0.89 mm, and 0.89 mm. Moreover, the length of the inner cylinder is 6.45 mm and its radius is 0.14 mm. The gap between the inner surface of the ellipsoid shell and the outer surface of the inner cylinder is proportional to the root of the mass ratio and the inner radius,^{18,35} which we calculated to be approximately 0.16 mm. Thus, the number of ions is estimated to be about $N_{\text{tot}} = 3.3 \times 10^5$ with $N_{\text{tot,Mg}} = 2.9 \times 10^4$ and $N_{\text{tot,Cd}} = 3.0 \times 10^5$. It is difficult to determine accurately the number of each type of ion species under the present conditions owing to the large total volume of the ions. There were some dark ions in the crystal whose species were not identified. Because the dark ions can be confined in the trap, their masses should be close to those of Mg^+ and Cd^+ . According to the literature,³⁰ the dark ions could be MgH^+ . We have ignored the dark ions in estimating the total number of ions.

To get insight into the separation of the two ion species, Figures 3(a)–(c) show the complete spatial separation between $^{24}\text{Mg}^+$ and $^{113}\text{Cd}^+$. These images were taken without optical filters. In Figs. 3(a) and 3(b), the 214.5 nm laser was tuned to brighten the bottom and upper parts of Cd^+ , respectively. In Fig. 3(c), the profile of Mg^+ in the core is clear. These were taken with an integration time of 3 s. In the same photograph, the profile of Cd^+ is fuzzy owing to chromatic aberration. Figure 3(d) shows a small Mg^+ ion crystal that has crystallized well. This image was taken using a 280 nm optical filter.

Although the first-order Doppler effect is suppressed owing to the Lamb–Dicke criterion, the SODFS is not negligible for microwave clocks based on ions. Lowering the temperature helps to reduce the SODFS. Hence, we measured the temperature of the ions for different values of V_{RF} and U_{End} . The results are shown in Figs. 4 and 5, respectively. Figure 4 shows the temperature dependence of outer-shell SC ions on the trapping voltage V_{RF} . All the data for this figure were measured for the same multi-component crystal in a single loading. Each point is the average of three measurements to ensure that equilibrium has been reached. Each error bars is the maximum difference between the three measurements in that set. After preparing a large multi-component crystal, we tuned the trapping voltages in a small range. For each value of U_{End} , we measured the ions temperature by changing V_{RF} in two opposite directions. The blue squares represent stepping up V_{RF} from a low level to a high level, and the red triangles

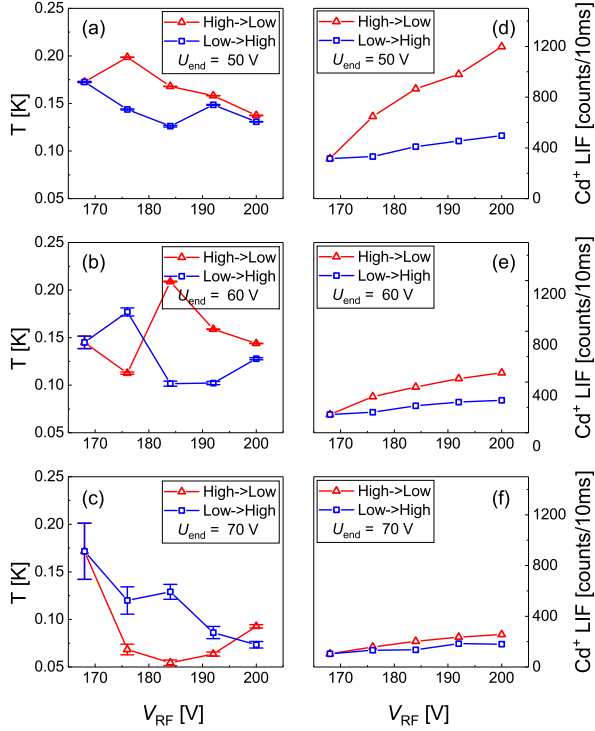


FIG. 4. The trapping RF voltage V_{RF} affects the SC efficiency. The graphs show the temperature of Cd^+ while the RF voltage are scanned for different end-cap voltages. Panels (a)-(c) show the variation of temperature with RF voltage, while (d)-(f) show the LIF signal intensity for these detections.

correspond to stepping down V_{RF} . The maximum measured temperature was about 200 mK, and the minimum temperature was on the order of 10 mK.

In Figures 4(a)-(c), we can see that there is no simple correlation between the ion temperature and V_{RF} . For example, the ion temperature could descend, ascend, and then descend again as V_{RF} increases. Thus, the ion temperature may vary with V_{RF} in different ways. The dependence of the ion temperature on V_{RF} strongly depends on the RF heating effect and the number of ions. The RF heating effect is due to ion-ion interactions during which micromotion energy is transferred to secular energy. Conversely, the RF heating depends on the ion temperature.³⁶ For example, in mono-component Mg^+ crystals, the RF heating rate is relatively low when the ion temperature is below 0.5 K, but increases rapidly when the ion crystal undergoes a phase transition.^{36,37} It is unclear how the RF heating affects the temperature of a large multi-component plasma (with up to 10^5 ions).³⁸ However, it is clear that the ion-ion Coulomb collision rate decreases both at high and low temperatures.³⁶ When ions temperature decreases, the amount of heat exchanged between the two components decreases, which decreases the efficiency of both the RF heating and SC. However, the rates at which the RF heating and SC efficiencies fall could be different. Thus, the irregular changes in the ion temperature in Fig. 4 might be caused by competition between RF heating and SC, or a structural phase transition.

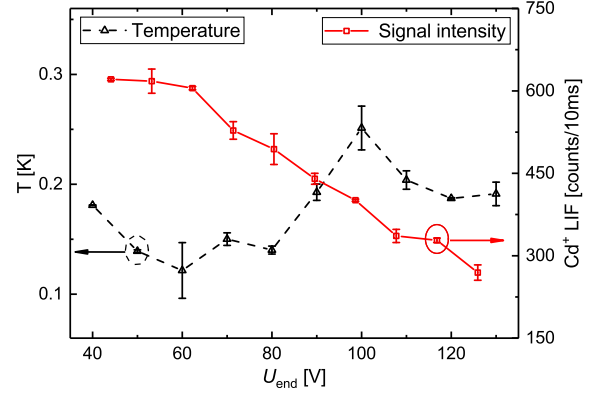


FIG. 5. End-cap voltage U_{End} affects the SC efficiency. The RF voltage V_{RF} is fixed at 200 V.

In addition, the number of ions decreases with time, which results in a collective decrease in signal intensity. This is even for the same probe laser intensity, as shown in Figs. 4(d)-(f). The ion density depends on the RF voltage for the same U_{End} value. Thus, the fluorescence counts increase as V_{RF} increases. However, a lower number of ions does not correspond to a lower temperature owing to the competition between RF heating and SC, as shown in Figs. 4(c) and 4(f). More importantly, the nonlinear resonance effects in a linear Paul trap with circular (rather than hyperbolic) electrodes are not negligible,³⁹ like the nonlinear resonance due to Coulomb interactions among ions.

The ion temperature dependence on U_{End} is shown in Fig. 5. The black triangles represent temperatures, and the red squares represent fluorescence count for varying U_{End} . Because of the Coulomb interaction with SC and the unbalanced radiation pressure of the cooling laser, the ion temperature decreases and then increases as U_{End} increases. The minimum temperature is at 60 V. A similar phenomenon has been observed for a small mono-component ion crystal (with 34 Ca^+ ions).⁴⁰ The spatial radius of each Ca^+ ion also reaches a minimum at a relatively low voltage. In Fig. 5, the number of trapped ions decreases as U_{End} increases, leading to a decrease in the signal intensity. Hence, the temperature for a relatively high U_{End} (>100 V) again decreases.

An accurate evaluation of the SODFS would require MD simulations from which the ion velocity distribution could be extracted. However, it can be roughly estimated using simple models for microwave ion clocks. The total SODFS due to both the secular motion and the micromotion of trapped ions is estimated as⁴¹

$$\frac{\Delta f}{f_0} = \left\langle -\frac{E_{Kinetic}}{Mc^2} \right\rangle = -\frac{3}{2} \frac{kT}{Mc^2} \left[1 + \frac{2}{3} (N_d^K) \right], \quad (3)$$

where f_0 is the central frequency, and N_d^K is the SODFS coefficient due to the micromotion averaged across the whole ion cloud. The temperature of $^{113}Cd^+$ decreases from 6 ± 1 K¹² to 0.20 ± 0.05 K, which reduces the SODFS from 1.88×10^{-14} to 6.26×10^{-16} . Moreover, the uncertainty for this shift also decreases from 0.31×10^{-14} to 1.57×10^{-16} .

For a cadmium ion microwave clock, dead time is unavoidable during interrogation, hence the Dick effect degrades the short-term frequency stability. With the SC method, the dead time can be reduced because no additional cooling step is needed. Thus, the Dick-effect-limited Allan deviation falls from $4 \times 10^{-13}/\sqrt{\tau}$ to $2 \times 10^{-13}/\sqrt{\tau}$ if the same local oscillator and microwave synthesizer are used, as in Zhang *et al.*¹³ In addition, illumination by a 280 nm laser could cause an AC Stark shift of the hyperfine clock transition. Fortunately, this can be controlled to be as low as the fluorescence by making the beam thin enough.⁴²

In summary, we produced a large SC ion crystal with up to 3.3×10^5 ions and a large mass ratio of 4.71 in a Paul trap. And we measured its temperature. The current mass ratio is based on the obtainable laser wavelengths, without optimization. We obtained a lower temperature for the outer shell even with a larger mass ratio. However, there is no clear definition of SC efficiency. It can intuitively be qualified by the mass ratio, the acquired temperature, and the total number of SC ions. This is the lowest directly measured temperature for such a large number of outer-shell SC ions with such a high mass ratio. These results confirm the translational temperature obtained by MD simulations. The SODFS of $^{113}\text{Cd}^+$ was reduced by two orders of magnitude and the Dick-effect-limited Allan deviation was halved under the same conditions as in our previous research.¹³ These results may be important in building a SC Cd^+ microwave frequency standard and useful for research on the SC of large ion crystals.

ACKNOWLEDGMENTS

This work was supported by the National Key R&D Program of China (2016YFA0302101) and the Initiative Program of State Key Laboratory of Precision Measurement Technology and Instruments.

- ¹N. Huntemann, C. Sanner, B. Lipphardt, C. Tamm, and E. Peik, *Phys. Rev. Lett.*, 116(6):063001 (2016).
- ²J. S. Chen, S. M. Brewer, C. W. Chou, D. J. Wineland, D. R. Leibbrandt, and D. B. Hume, *Phys. Rev. Lett.*, 118(5):053002 (2017).
- ³N. Deb, L. L. Pllum, A. D. Smith, M. Keller, C. J. Rennick, B. R. Heazlewood, and T. P. Softley, *Phys. Rev. A*, 91(3):033408 (2015).
- ⁴J. Biesheuvel, J. P. Karr, L. Hilico, K. S. E. Eikema, W. Ubachs, and J. C. J. Koelemeij, *Nat. Commun.*, 7:10385 (2016).
- ⁵J. Zhang, G. Pagano, P. W. Hess, A. Kyprianidis, P. Becker, H. Kaplan, A. V. Gorshkov, Z. X. Gong, and C. Monroe, *Nature*, 551(7682):601 (2017).
- ⁶N. Huntemann, B. Lipphardt, C. Tamm, V. Gerginov, S. Weyers, and E. Peik, *Phys. Rev. Lett.*, 113(21):210802 (2014).
- ⁷S. Willitsch, *Int. Rev. Phys. Chem.*, 31(2):175–199 (2012).
- ⁸S. Mulholland, H. A. Klein, G. P. Barwood, S. Donnellan, D. Gentle, G. Huang, G. Walsh, P. E. G. Baird, and P. Gill, *arXiv:1811.06421 (preprint)*, 2018.
- ⁹P. D. D. Schwindt, Y. Y. Jau, H. L. Partner, D. K. Serkland, A. Ison, A. McCants, E. Winrow, J. Prestage, J. Kellogg, N. Yu, et al. In *2015 Joint Conference of the IEEE International Frequency Control Symposium & the European Frequency and Time Forum*, pages 752–757. IEEE, 2015.
- ¹⁰G. K. Gulati, S. Chung, T. Le, J. Prestage, L. Yi, R. Tjoelker, N. Nyu, and C. Holland, In *2018 IEEE International Frequency Control Symposium (IFCS)*, pages 1–2. IEEE, 2018.
- ¹¹A. Todd, E. A. B. Ely, J. D. Prestage, J. M. Seubert, and R. L. Tjoelker, *IEEE Trans. Ultrason. Ferroelectr. Freq. Control*, 65(6):950–961 (2018).
- ¹²K. Miao, J. W. Zhang, X. L. Sun, S. G. Wang, A. M. Zhang, K. Liang, and L. J. Wang, *Optics Lett.*, 40(18):4249–4252 (2015).
- ¹³J. W. Zhang, K. Miao, and L. J. Wang, *Chin. Phys. Lett.*, 32(1):010601 (2015).
- ¹⁴G. J. Dick, J. D. Prestage, C. A. Greenhall, and L. Maleki, Technical report, California Inst of Technology, Pasadena Jet Propulsion Lab, 1990.
- ¹⁵R. E. Drullinger, D. J. Wineland, and J. C. Bergquist, *Appl. Phys.*, 22(4):365–368 (1980).
- ¹⁶S. Knünz, M. Herrmann, V. Batteiger, G. Saathoff, T. W. Hänsch, and Th. Udem, *Phys. Rev. A*, 85(2):023427 (2012).
- ¹⁷J. Zhang, K. Miao, L. Wang, and X. Sun, In *2015 Joint Conference of the IEEE International Frequency Control Symposium & the European Frequency and Time Forum*, pages 758–760. IEEE, 2015.
- ¹⁸L. Hornekær, Ph.D. thesis (University of Aarhus, 2000).
- ¹⁹M. A. Van Eijkelenborg, M. E. M. Storkey, D. M. Segal, and R. C. Thompson, *Phys. Rev. A*, 60(5):3903 (1999).
- ²⁰T. Hasegawa and T. Shimizu, *IEEE Trans. Instrum. Meas.*, 50(2):556–558 (2001).
- ²¹D. Offenberg, C. B. Zhang, Ch. Wellers, B. Roth, and S. Schiller, *Phys. Rev. A*, 78(6):061401 (2008).
- ²²D. J. Larson, J. C. Bergquist, J. J. Bollinger, W. M. Itano, and D. J. Wineland, *Phys. Rev. Lett.*, 57(1):70 (1986).
- ²³H. Imajo, K. Hayasaka, R. Ohmukai, U. Tanaka, M. Watanabe, and S. Urabe, *Phys. Rev. A*, 53(1):122 (1996).
- ²⁴H. Imajo, K. Hayasaka, R. Ohmukai, U. Tanaka, M. Watanabe, and S. Urabe, *Phys. Rev. A*, 55(2):1276 (1997).
- ²⁵D. R. Denison, *J. Vacuum Sci. Technol.*, 8(1):266–269 (1971).
- ²⁶W. Paul, *Rev. Mod. Phys.*, 62(3):531 (1990).
- ²⁷W. C. Martin and R. Zalubas, *J. Phys. Chem. Ref. Data*, 9(1):1–58 (1980).
- ²⁸D. L. Moehring, B. B. Blinov, D. W. Gidley, R. N. Kohn Jr., M. J. Madsen, T. D. Sanderson, R. S. Vallery, and C. Monroe, *Phys. Rev. A*, 73(2):023413 (2006).
- ²⁹M. Drewsen, I. Jensen, J. Lindballe, N. Nissen, R. Martinussen, A. Mortensen, P. Staunum, and D. Voigt, *Int. J. Mass Spectrom.*, 229(1–2):83–91 (2003).
- ³⁰K. Mølhave and M. Drewsen, *Phys. Rev. A*, 62(1):011401 (2000).
- ³¹R. Fritz, In *Frequency standards: basics and applications*, pages 149–153. John Wiley & Sons, 2006.
- ³²R. B. Warrington, P. T. H. Fisk, M. J. Wouters, M. A. Lawn, *IEEE Trans. Ultrason. Ferroelectr. Freq. Control*, 49(8):1166–1174 (2002).
- ³³D. Michael, H. Liv, K. Niels, M. Kristian, T. Anne-Marie, V. Zelinda, M. Anders, J. Frank, In *AIP Conference Proceedings*, 606(1):135–144 (2002).
- ³⁴L. Hornekær, N. Kjærgaard, A. M. Thommesen, and M. Drewsen, *Phys. Rev. Lett.*, 86(10):1994 (2001).
- ³⁵T. M. O’Neil, *Phys. Fluids*, 24(8):1447–1451 (1981).
- ³⁶V. L. Ryjkov, X. Zhao, and H. A. Schuessler, *Phys. Rev. A*, 71(3):033414 (2005).
- ³⁷X. Zhao, V. L. Ryjkov, and H. A. Schuessler, *Phys. Rev. A*, 73(3):033412 (2006).
- ³⁸L. Hornekær and M. Drewsen, *Phys. Rev. A*, 66(1):013412 (2002).
- ³⁹R. Takai, K. Nakayama, W. Saiki, K. Ito, and H. Okamoto, *J. Phys. Soc. Jpn.*, 76(1):014802–014802 (2007).
- ⁴⁰K. Okada, M. Wada, T. Takayanagi, S. Ohtani, and H. A. Schuessler, *Phys. Rev. A*, 81(1):013420 (2010).
- ⁴¹J. D. Prestage, R. L. Tjoelker, L. Robert, and L. Maleki, In *Proceedings of the 1999 Joint Meeting of the European Frequency and Time Forum and the IEEE International Frequency Control Symposium (cat. No. 99CH36313)*, pages 121–124. IEEE, 1999.
- ⁴²Y. N. Zuo, K. Miao, C. Gao, J. W. Zhang, and L. J. Wang, In *2016 IEEE International Frequency Control Symposium (IFCS)*, pages 1–4. IEEE, 2016.